Size-Dependent Oscillatory Magnetoresistance in Cadmium*†

P. D. Hambourger‡ and J. A. Marcus
Department of Physics, Northwestern University, Evanston, Illinois 60201
(Received 6 November 1972)

Size-dependent oscillations in the magnetoresistance and Hall effect in cadmium have been studied using the field-modulation method. Nine sets of oscillations were observed for the first time and three sets discovered previously were observed with greater resolution over a larger range of field orientations. Most of the oscillations are assigned to orbits on the second-band "monster" and third-band "lens" sheets of the Fermi surface. The results indicate a slight departure of the lens from axial symmetry. Considerable second-harmonic content was observed on some of the oscillations. Disappearance of some monster oscillations but not the lens oscillations in magnetic fields greater than 8 kOe is attributed to the effect of magnetic breakdown of the energy gap between the first and second bands. Results are discussed in terms of the size-effect theory of Bloomfield and the Fermi-surface model of Stark and Falicov.

I. INTRODUCTION

Oscillations in the low-temperature galvanomagnetic properties of metallic samples with parallel opposing faces have been observed in several metals. This effect, produced by Fermi-surface electrons which travel across the sample without scattering, was originally predicted by Sondheimer,[1] who considered the free-electron case and showed that oscillations arise from electrons at the "limiting points"[2] of the Fermi surface. The limiting-point oscillations were first observed in sodium by Babiskin and Seibenmann[3] and have been investigated in cadmium by Zebouni *et al.*,[4] Grenier *et al.*,[5] and Mackey *et al.*[6] Gurevich[7] showed that similar oscillations occur for an arbitrary Fermi surface and field orientation if the time-averaged component of the electron quasimomentum along the magnetic field direction has a discontinuity or extremum. Oscillations of this type were first observed by Munarin and Marcus[8] in gallium and were detected over a small range of field orientations in cadmium by Grenier *et al.*,[5] who also studied the problem theoretically and pointed out that these oscillations arise if the Fermi-surface geometry is such that there is an extremum or discontinuity in the orbital-area derivative $\partial A/\partial k_{\hat{z}}$ (where $\hat{z}$ represents the magnetic field direction) evaluated at the Fermi surface.

A more general and detailed theory of the size-dependent galvanomagnetic oscillations has been developed by Bloomfield,[9,10] and compared with experimental results on gallium by Munarin, Marcus, and Bloomfield.[10] The data were found to be in general agreement with the theory, although the comparison was hampered by the lack of a sufficiently detailed model of the highly complicated gallium Fermi surface.

Cadmium is well suited to size-effect studies because it is available in high purity and its Fermi surface is well understood. We have made an investigation of the size-dependent magnetoresistance and Hall effect in cadmium[11] using the field-modulation method and have observed twelve sets of oscillations, including three of the four sets observed by other workers in the dc transport properties[4-6,12] and rf surface impedance.[13-15] We have assigned ten of the twelve periods to orbits on the Fermi surface and find that our results are in agreement with Bloomfield's predictions provided appropriate modifications are made to account for the influence of magnetic breakdown.

The theory of the oscillatory galvanomagnetic effect and the Fermi surface of cadmium are discussed in Sec. II. The experimental procedure is described in Sec. III, and the data are presented and discussed in Sec. IV.

II. THEORY

Oscillatory Effect

The sample geometry for observation of this size effect is shown in Fig. 1. The oscillations arise from electrons at the Fermi surface which travel across the sample without scattering and suffer diffuse reflection at the faces. The trajectory followed by an electron is in general a distorted helix extending parallel to the magnetic field. Elementary consideration of the perturbation of the trajectory by an applied electric field indicates that the net current transported by the electron averages to zero over each complete revolution.[16] If, however, there are a nonintegral number of turns in the trajectory from one face to the other, a net transport of current results. Since the cyclotron frequency is proportional to the magnetic field strength while the average component of drift velocity parallel to the field is constant, the "helix" tightens with increasing magnetic field and the sample resistance goes through one cycle of oscillation for each turn added to the trajectory.

The number of turns in the helix is given by the

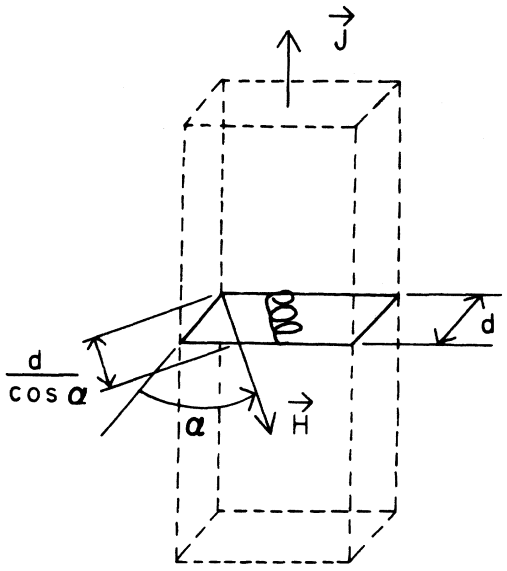

FIG. 1. Electron trajectories responsible for oscillatory magnetoresistance.

product of drift time and cyclotron frequency:

$$N(H)=\frac{d}{\langle v_z\rangle\cos\alpha}\,\frac{eH}{2\pi m^*c}\ , \tag{1}$$

where $\langle v_z\rangle$ is the component of the velocity along $\vec{H}$ averaged over one cyclotron period, m^* is the cyclotron effective mass, and α is the angle between $\vec{H}$ and the normal to the flat faces. The oscillations therefore are periodic in H with period given by

$$P=2\pi m^*c\langle v_z\rangle(ed)^{-1}\cos\alpha\ . \tag{2}$$

The period is related to the geometry of the Fermi surface since[17]

$$m^*\langle v_z\rangle=\frac{\hbar}{2\pi}\frac{\partial A}{\partial k_z}\ . \tag{3}$$

In general, the oscillatory contributions from electrons on different Fermi-surface orbits average to zero, but finite contributions arise from electrons at regions of the surface where $\partial A/\partial k_z$ is extremal, constant, or discontinuous as a function of k_z, as well as from electrons at the limiting points. The observed oscillatory period will then be

$$P=\frac{\hbar c\cos\alpha}{ed}\left|\frac{\partial A}{\partial k_z}\right|_{k_{z0}}\ , \tag{4}$$

where k_{z0} indicates the location of the extremum, discontinuity, limiting point, or region of constant $\partial A/\partial k_z$. In the case of an axially symmetric limiting point, it can be shown that

$$\left|\frac{\partial A}{\partial k_z}\right|_{k_{z0}}=2\pi R\ , \tag{5}$$

where R is the radius of curvature. In the more general case of an elliptic limiting point, R is replaced by $(R_1R_2)^{1/2}$, where R_1 and R_2 are the principal radii of curvature at the limiting point.

The nature of the orbit giving rise to a given set of oscillations can, in principle, be determined from the magnetic field dependence of the amplitude.[10] However, since the voltages measured experimentally are proportional to the sample resistivity rather than the conductivity, the recorded amplitudes will be influenced by the *monotonic* galvanomagnetic properties of the metal and will therefore depend on its state of compensation and the presence or absence of open orbits. In Table I we summarize Bloomfield's[10] predictions for the amplitude of the oscillations in the transverse magnetoresistance ($\vec{H}\perp\vec{J}$) of a compensated metal having no open orbits, the case which applies to cadmium for most field orientations.[18]

Nonsinusoidal oscillation wave shapes have been predicted on the basis of two different mechanisms. Bloomfield[10] has shown that the oscillations will be distorted if the orbit is noncircular, so the components of an electron's velocity normal to the magnetic field are not sinusoidal functions of its displacement along $\vec{H}$. The frequency spectrum of the oscillations will then consist of a fundamental and a series of harmonic terms. Mackey and Sybert[19,20] and Soffer[21] predict that harmonics will arise if some electrons undergo specular reflection at the sample faces, provided the Fermi surface has axial symmetry about the normal to the faces and $\vec{H}$ is along this normal. According to their calculations, an electron that makes, say, two trips across the sample before suffering diffuse reflection would contribute to the conductivity in the same way an an electron making one trip across a sample twice as thick. We would then expect a series of harmonics with amplitudes dependent on the probability of specular reflection.

Fermi Surface of Cadmium

The Fermi surface and electronic properties of cadmium have been studied in considerable detail by several different methods.[18,22,23] Stark and

TABLE I. Theoretical magnetic field dependence of amplitude of transverse-magneoresistance oscillations in a compensated metal with no open orbits.[a]

Type of orbit	Field dependence of amplitude
$\partial A/\partial k_z$ constant	H^2
$\partial A/\partial k_z$ extremal	$H^{3/2}$
$\partial A/\partial k_z$ discontinuous	H^1
Limiting point	H^0

[a]Reference 10.

Falicov[24,25] have developed a remarkably accurate model of the Fermi surface using a pseudopotential approach. Extremal areas and caliper dimensions on this model are in excellent agreement with the results of accurate de Haas–van Alphen[22] and Gantmakher rf-size-effect[23] experiments (to within 1% in many cases).

A perspective drawing of the model is shown in Fig. 2. One-sixth of the Fermi surface has been omitted for clarity in (a) and (b). The first band contains six symmetry-related hole pockets centered at H and known as "caps." The second-band hole surface, known as the "monster," consists of six symmetry-related pieces which span the Brillouin zone from top to bottom and therefore support open orbits[18] parallel to [0001]. The monster is thus a set of undulating cyclinders of infinite length, each having threefold symmetry about [0001]. The third-band electron "lens" has nearly spherical surfaces except for slight rounding at the edge. Gantmakher-size-effect[26] and de Haas-van Alphen[25] experiments have not detected any significant departure from perfect axial symmetry about [0001].

The nearly-free-electron (NFE) model[17] contains electron "butterfly" and "cigar" surfaces in the third and fourth bands, respectively, while the calculation of Stark and Falicov[24] indicates that the relevant band minima are raised above the Fermi energy. There is little evidence to support the existence of these pieces. Naberezhnykh, Danshin, and Symbal[15] have observed weak rf-size-effect oscillations which they attributed to an extremal $\partial A/\partial k_z$ orbit on the butterfly, and Galkin *et al.*[27] have attributed weak magnetoacoustic resonances to this orbit. A search for the corresponding galvanomagnetic-size-effect oscillations, described in Sec. IV, proved fruitless.

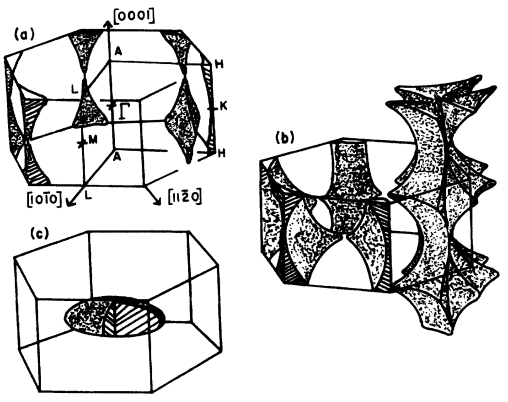

FIG. 2. Fermi surface of cadmium as calculated by Stark and Falicov (Ref. 25): (a) first band; (b) second band; (c) third band.

The energy gap between the first and second bands, arising entirely from the effect of spin-orbit coupling, is estimated to be only 0.07 eV.[22] Because of this small gap, magnetic-breakdown phenomena have been observed in moderate magnetic fields.[18,22,28] We find that magnetic breakdown has a profound effect on the amplitude of some sets of size-effect oscillations arising from orbits on the monster. These results are discussed in Sec. IV.

III. EXPERIMENTAL DETAILS

Six single-crystal samples approximately 3-mm wide, 15-mm long, and 0.8–1.5-mm thick were prepared from 99.9999%-pure cadmium obtained in the form of zone-refined bars from Cominco-American, Inc. Oriented parallelepipeds measuring $3\times3\times15$ mm were spark cut from the large crystals found in these bars and were reduced to the desired thickness by spark planing in such a way that the large faces were as flat and parallel as possible.[29] After cleaning in a saturated solution of chromic acid to remove the residue left by the spark planer,[30] the samples were lightly electropolished in a 57% solution of H_3PO_4 in water as described in Ref. 6. Polishing was carried out for just a few minutes on each surface, reducing the thickness by about 25 μm. While this certainly was insufficient to remove all damage left by the planer, we felt that a longer electropolish would do more harm than good by rounding the faces. The resulting surfaces showed reasonably good Laué back-reflection patterns and deviated from parallelism by less than 2 μm over the region near the center where the potential probes were attached. On most of the samples used for the final measurements, the normal to the plane faces lay within $\frac{1}{4}^\circ$ of a crystallographic axis so the angle α could be determined accurately from the symmetry of the data. Residual resistance ratios ($\rho_{300\text{ K}}/\rho_{4.2\text{ K}}$) ranged from 31 000 to 44 000 (not corrected for size effects).

Sample thicknesses were measured to ±3 μm by an instrument[29] which made use of the carriage assembly of a travelling microscope, mounted with the leadscrew vertical. The microscope tube was replaced by a mounting which held a Hewlett-Packard displacement transducer (linear differential transformer). The plunger (mass 2.4 g) of the transducer made contact with the sample, which was placed on a pedestal attached to the frame of the instrument. The thickness was determined from the leadscrew settings required for zero transducer output with and without the sample. In this way, the transducer was used as a null indicator so its slight nonlinearity did not affect the results. This method eliminated the uncertainty in matching a microscope crosshair to the sample

edges, which were somewhat irregular due to the electropolishing process.

The oscillatory part of the magnetoresistive or Hall voltage was detected by the audio-frequency field-modulation technique, using equipment similar to that described in Ref. 10. A direct current of 2.5 A was passed through the sample and the magnetic field was modulated by a parallel sinusoidal component of up to 600-Oe peak to peak at 50 Hz. The voltage appearing on the potential leads was fed to a PAR Model HR-8 lock-in amplifier tuned either to the second or seventh harmonic of the modulation frequency. Competing oscillatory periods were separated by means of the wide-amplitude modulation method described by Stark and Windmiller.[31]

Periods were determined from field sweeps and from field-rotation diagrams taken at constant field strength. For oscillations periodic in H, it can readily be shown[29] that one cycle of oscillation on a rotation diagram indicates a change in oscillation frequency of H^{-1}, where H is the strength of the steady magnetic field. Data generally were taken at a temperature of 1.3 K.

IV. RESULTS AND DISCUSSION

The oscillatory magnetoresistive voltages were typically on the order of 25–250 nV, implying resistivity changes of 10^{-9}–10^{-8} Ω cm. Two recorder tracings, taken at the same field orientation ($\vec{H} \parallel [0001]$) but with different modulation amplitude (H_1), are shown in Fig. 3. Each trace is dominated by one of the two fundamental periods observed at this orientation. These plots illustrate the two general types of amplitude behavior observed in this study. The long-period oscillations are nearly constant in amplitude over the entire field range of 1–15 kOe, while the short-period oscillations increase rapidly in amplitude up to about 9 kOe. The long-period oscillations were first observed by Zebouni *et al.*[4] and were assigned to the limiting point at the apex of the lens,[4–6] while the short-period oscillations were first observed by Grenier *et al.*,[5] who attributed them tentatively to an extremal $\partial A/\partial k_z$ orbit on the monster—an assignment confirmed by our data and examination of the Stark-Falicov model. Since the Fermi surface does not support open orbits for this field orientation, the field dependence of amplitude in both cases is in qualitative agreement with the predictions of Bloomfield (Table I). We have used the behavior of the amplitudes of the other oscillations as a guide in assigning them to orbits on the Fermi surface.

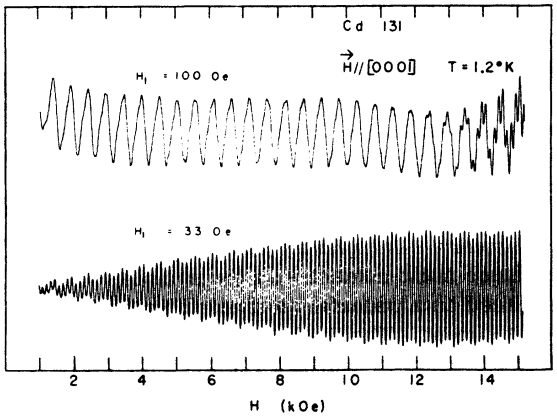

FIG. 3. Recorder tracings of oscillations taken at same field orientation with two different settings of modulation amplitude (H_1).

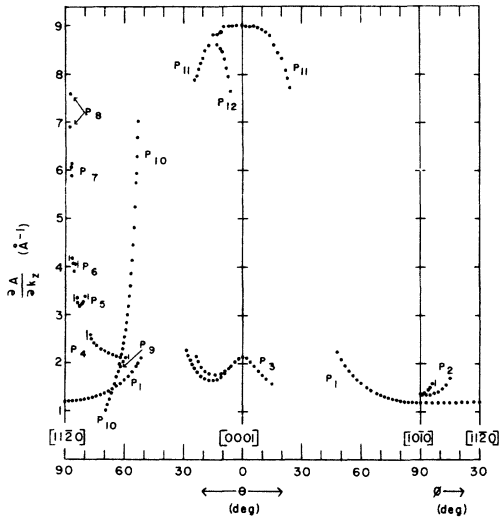

FIG. 4. Orientation dependence of extremal area derivatives obtained from oscillation periods. A vertical line at the end of a branch indicates the abrupt disappearance of the oscillations.

Periods and Orbit Locations

The orientation dependence of the area derivatives obtained from the period measurements is shown in Fig. 4. The field directions are in real space. θ is the angle between [0001] and $\vec{H}$, and ϕ is the angle between [10$\bar{1}$0] and the projection of $\vec{H}$ on the (0001) plane. All periods except P_1, P_3, and P_{11} were observed for the first time in this experiment. The results for P_1–P_5 are believed to be accurate to 1% or better; those for the remaining periods are accurate to 2% or better.

The P_1 oscillations arise from an area derivative extremum near the rim of the lens and were first observed in the rf surface impedance by Naberezhnykh and Maryakhin.[13] Our values for $\partial A/\partial k_z$ differ considerably from their results, being ~7% larger in the (0001) plane and ~25% larger for $\theta = 58°$ in the (10$\bar{1}$0) plane. The reason for this dis-

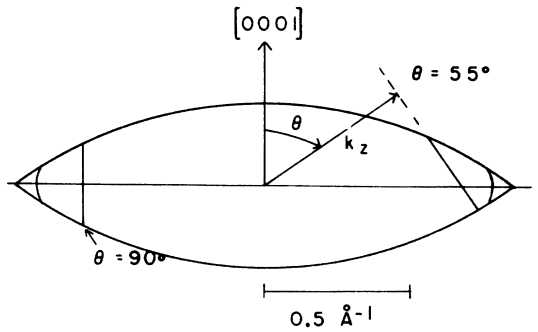

FIG. 5. Approximate locations of the P_1 orbit on the lens for two field orientations.

crepancy is not understood, but the close agreement we obtained between results from different samples lends support for our values. The approximate location of the orbit for two field orientations is shown in Fig. 5.

An interesting feature of our P_1 results is a small but clearly resolved departure from axial symmetry about [0001], as shown in Figs. 6 and 7. The results for $\theta = 55°$ in the $(10\bar{1}0)$ and $(11\bar{2}0)$ planes (Fig. 6) differ by 4%. The data for the (0001) plane (Fig. 7) are particularly convincing, although the anisotropy in this plane is only 1%, because the high symmetry permits four separate measurements of $\partial A/\partial k_z$ in the same sample for most values of ϕ. Apparently there is a slight "fluting" of the lens that has a significant effect on the extremal area derivative but negligible effect

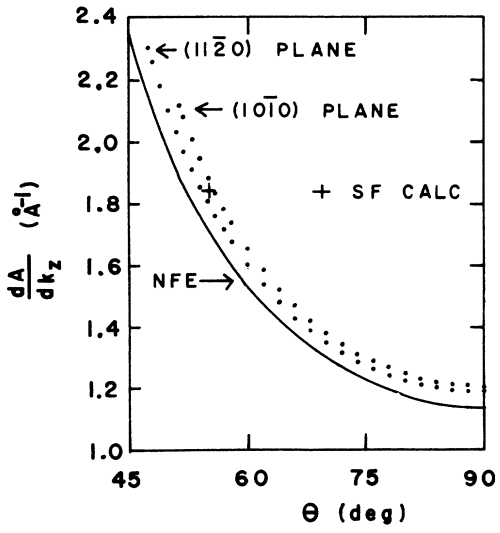

FIG. 6. Orientation dependence of extremal area derivative for the lens. Dots: P_1 data. Smooth curve: nearly-free-electron model. (+) Stark-Falicov calculation.

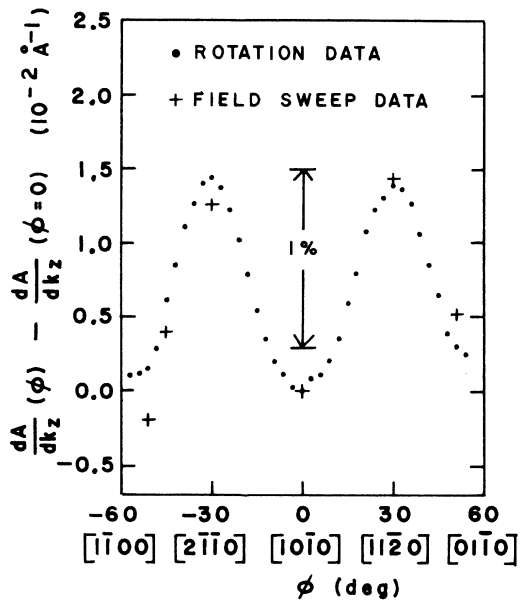

FIG. 7. Anisotropy of extremal area derivative for the lens with $\vec{H}$ in the (0001) plane, determined from P_1.

on the extremal-orbit areas and calipers measured by the de Haas–van Alphen effect and Gantmakher effect, respectively. The curve labeled NFE in Fig. 6 shows the extremal area derivative calculated from the NFE model. [NFE values from the $(10\bar{1}0)$ and $(11\bar{2}0)$ planes are, of course, identical.] The point labeled "SF" was calculated by Stark[25] from the Stark-Falicov model. His calculated values for the $(10\bar{1}0)$ and $(11\bar{2}0)$ planes are almost identical and lie halfway between the experimental points.

P_2 consists of two branches which cross at $[10\bar{1}0]$, the upper branch disappearing abruptly at $\phi = 6°$. The oscillations were observed when $\vec{H}$ was tilted a few degrees out of the (0001) plane but were too weak to be measured. P_2 arises from orbits around the "ears" of the monster, as shown in Fig. 8. According to the Stark-Falicov model, the extremal $\partial A/\partial k_z$ orbits pass over or near the tips of the ears as indicated by arrows in the figure. The two orbits are identical when $\vec{H}$ is along $[10\bar{1}0]$, accounting for the crossing of the branches. As ϕ increases, one extremal orbit moves farther into the crevice between the ears until it becomes open along [0001], eliminating the extremum in $\partial A/\partial k_z$ and the upper-branch oscillations.

We attribute the P_3 oscillations to orbits on the monster, as first suggested by Grenier *et al.*[5] On the Stark-Falicov model, two extremal $\partial A/\partial k_z$ orbits encircle the monster slightly above and below the ΓKM plane. These orbits are identical by symmetry only when $\vec{H}$ lies in the $(11\bar{2}0)$ plane, accounting for the observed splitting of P_3 with $\vec{H}$ in

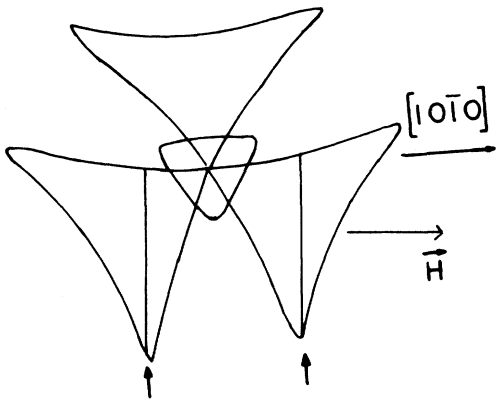

FIG. 8. Locations of the P_2 orbits on the monster.

the (10$\bar{1}$0) plane. {P_3 actually separated into two periods differing by ~ 1% as the field was rotated away from [0001] in the (11$\bar{2}$0) plane. This could be accounted for by a slight sample misalignment which could cause the plane of field rotation to deviate from the plane of symmetry.} For $\vec{H} \parallel [0001]$ we find $\partial A/\partial k_z = 2.15$ Å^{-1}, about 5% larger than the result of Grenier *et al.* but within 0.5% of the value obtained more recently by Mackey, Sybert, and Waller, [12] who observed the oscillations using an eddy-current method.

P_4–P_8 appear over small but sharply defined ranges of field orientation in the (10$\bar{1}$0) plane. There is a correlation between the angles at which these oscillations disappear and the location of anomalies in the *monotonic* magnetoresistance. This is shown in Fig. 9, where we plot the total sample resistivity, as measured by the usual dc method, against magnetic field direction and indicate the ranges over which size-effect oscillations were observed by the modulation technique. Many of the magnetoresistance anomalies were first observed by Tsui and Stark, [32] who showed that they

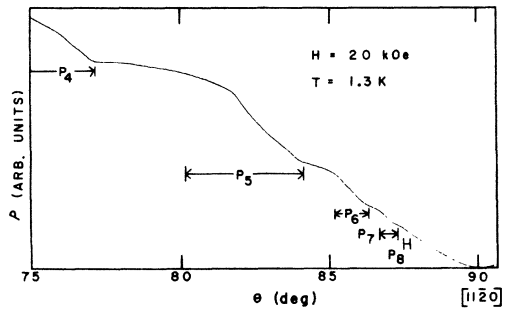

FIG. 9. Rotation diagram of the *monotonic* transverse magnetoresistance with $\vec{H}$ in the (10$\bar{1}$0) plane. Brackets indicate the ranges over which size-effect oscillations were detected by the modulation method.

are associated with the onset of various extended orbits on the monster as $\vec{H}$ is rotated away from [0001]. For example, the kink at $\theta = 77°$ marks the disappearance of a single-zone orbit centered near the ΓKM plane and its replacement by an extended orbit passing through parts of three Brillouin zones. We therefore infer that P_4 arises from a single-zone orbit centered near the ΓKM plane since its cutoff coincides with the disappearance of this orbit. The kink at $\theta = 84°$ is associated with the disappearance of a two-zone orbit centered near the AHL plane and its replacement by a four-zone orbit, implying that P_5 arises from the two-zone orbit. In similar fashion we deduce the nature of the orbits giving rise to P_6–P_8. The approximate locations of the orbits are shown in Fig. 10.

Although P_9 appears to join P_4 near $\theta = 59°$, where P_4 disappears, we could not confirm this because the P_4 and P_9 oscillations damp out at $H \approx 8$ kOe at this orientation because of magnetic-breakdown effects. No definite orbit assignment was found for P_9, but the similarity of the damping of P_4 and P_9 at higher magnetic fields suggests that P_9 arises from an orbit on the monster near that giving rise to P_4.

P_{10} is distinguished by the rapid change of $\partial A/\partial k_z$ with field orientation. An orbit having this characteristic passes around one ear of the monster as shown in Fig. 11. For such an orbit, $\partial A/\partial k_z$ increases as $\vec{H}$ is rotated toward [0001], becoming extremely large as the orbit plane approaches tangency to the Fermi surface. A graph-

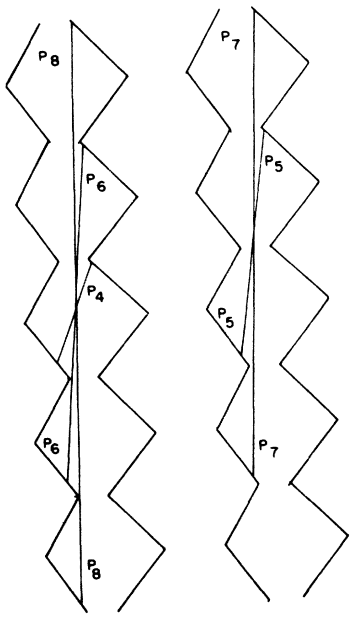

FIG. 10. Approximate locations of the P_4–P_8 orbits on the monster.

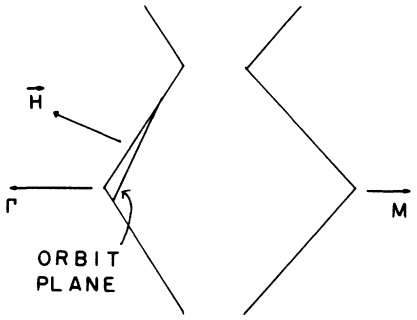

FIG. 11. Approximate location of the P_{10} orbit on the monster.

ical check of the Stark-Falicov model showed that $\partial A/\partial k_z$ is in fact extremal for this orbit and that the orientation dependence is in qualitative agreement with the data.

P_{11} and P_{12} exhibit the field-independent amplitude characteristic of limiting-point oscillations. P_{11} arises from electrons at the apex of the lens and is discussed in detail in Refs. 4–6. For $\vec{H} \| [0001]$, our data indicate a radius of curvature of 1.43 Å^{-1}, in good agreement with the results of Mackey, Sybert, and Waller[12] and about 1.4% larger than the NFE lens radius. We observed the oscillations out to $\theta = 25°$ in the $(10\bar{1}0)$ and $(11\bar{2}0)$ planes. There is considerable scatter in the data for $\theta > 8°$ because of interference from P_{12} in the $(10\bar{1}0)$ plane and from an unknown period in the $(11\bar{2}0)$ plane (resolution was reduced because of the long periods of P_{11} and P_{12}, ~400 Oe). We find that the P_{11} data for the two planes are identical to within an uncertainty of ± 2%.

No assignment was found for P_{12}. These oscillations produce a strong beat pattern with P_{11} and probably arise from a limiting point because they appear to have constant amplitude. P_{12} was observed in both samples in which this region was studied, making an explanation in terms of crystal microstructure implausible. The smooth surfaces of the cap or monster might conceivably support a limiting-point "orbit," but examination of the Fermi surface indicates that this could occur only for much larger values of θ. Evidence of beating observed with $\vec{H}$ in the $(11\bar{2}0)$ plane suggested the presence of a branch similar to P_{12}, but the oscillations were too weak to study.

We have made a careful search for short-period galvanomagnetic oscillations corresponding to a set of weak oscillations observed in the perpendicular-field rf size effect with $\vec{H} \| [0001]$ by Naberezhnykh, Danshin, and Symbal,[15] who attributed these oscillations to an orbit on the hypothetical third-band butterfly surface of the NFE model. The modulation amplitude was adjusted to maximize the sensitivity for the expected period of ~13 Oe while severely attenuating the longer-period P_3 and P_{11} signals, and data were taken at relatively low fields (1–3 kOe) to avoid smearing of the short-period oscillations by surface irregularities. No oscillations were detected in the magnetoresistance or Hall effect.

The results for some of the more prominent oscillations are summarized in Table II.

Harmonics

Some of the oscillations were found to have considerable second-harmonic content (period one-half that of the fundamental), but no higher harmonics were observed. Figure 12 shows a recorder tracing of the P_4 oscillations with the second harmonic clearly visible. In this case the field-modulation amplitude was chosen to enhance the second harmonic by a factor of approximately 2.7 relative to the fundamental. By appropriate adjustment of the modulation,[31] it was possible at many orientations to select and record the fundamental and harmonic components separately. In this way, the second harmonics of P_3–P_5, P_9, and P_{11} were observed while no harmonic content was detected on P_1. The other oscillations were much weaker and were not checked for harmonics. P_4 and P_9 showed the strongest harmonic content; the amplitude of the second harmonic was 15–40% as large as the amplitude of the fundamental, depending on field orientation. P_{11} showed ~15% second-harmonic content with $\vec{H}$ simultaneously parallel to [0001] and the normal to the plane faces of the sample. At $\theta = 5°$ the harmonic content was nearly as large as at $\theta = 0°$.

We attribute the harmonic content of P_3–P_5 and P_9 to the complicated noncircular geometry of the monster orbits, rather than to specular reflection, because the orbits are not axially symmetric and the harmonic is observed for arbitrary field orientations with respect to the sample normal.[10] Our failure to detect the second harmonic of P_1 is consistent with this interpretation since the relatively simple shape of the lens orbit implies that the higher-order coefficients in the Fourier expansion of the electron velocity[10] are smaller for this orbit.

TABLE II. Summary of major experimental area derivatives and their orbit assignments.

Period	Assignment	Field direction	$\partial A/\partial k_z$ (Å^{-1})
P_1	lens	$[10\bar{1}0]$	1.19
P_1	lens	$[11\bar{2}0]$	1.20
P_1	lens	$\theta = 52°$, $\phi = 0°$	1.97
P_1	lens	$\theta = 52°$, $\phi = 30°$	2.08
P_2	monster	$[10\bar{1}0]$	1.37
P_3	monster	[0001]	2.15

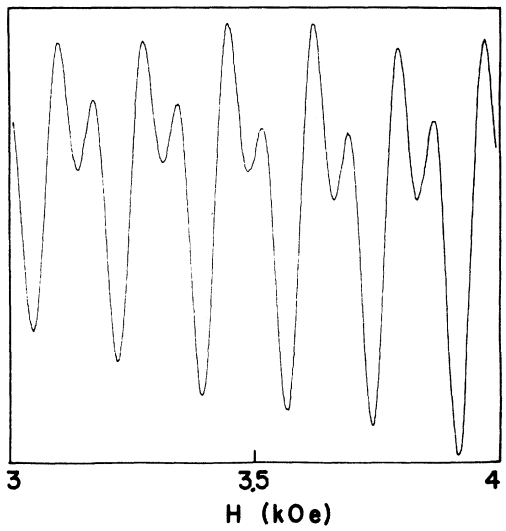

FIG. 12. Recorder tracing of the P_4 oscillations exhibiting second-harmonic content. The second harmonic has been enhanced by a factor of 2.7 relative to the fundamental by the choice of field-modulation amplitude.

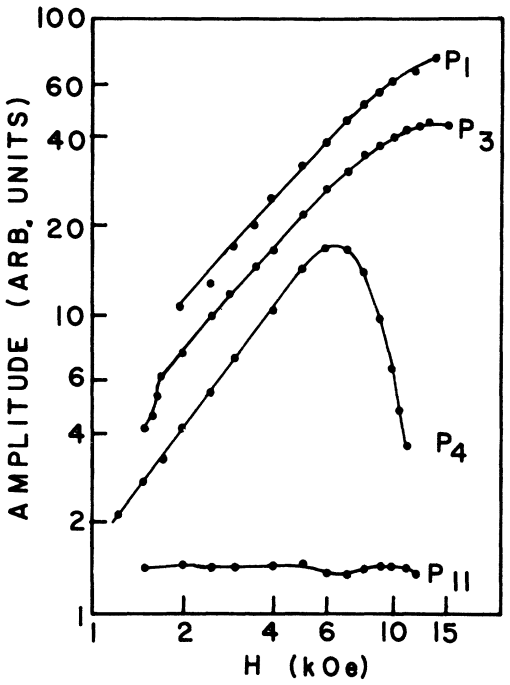

FIG. 13. Variation of oscillation amplitude with magnetic field strength for several sets of oscillations. Smooth curves are drawn by eye through the data points. Curves have been shifted vertically to separate them.

The harmonic content of P_{11} may arise from specular reflection, at least when $\vec{H}$ is along [0001], because then the Fermi surface is axially symmetric about the limiting point. Schwarz[33] also has observed the second harmonic of the limiting-point oscillations and has found evidence of a correlation between harmonic amplitude and sample surface condition.

Amplitudes—Magnetic Breakdown

Representative plots of amplitudes vs magnetic field are shown in Fig. 13. The amplitude of P_{11} is essentially constant, as expected for limiting-point oscillations in a compensated metal. The amplitudes of P_1 and P_3 increase with field over most of the range, although not as rapidly as the $H^{3/2}$ power law predicted by Bloomfield for an extremal $\partial A/\partial k_z$ orbit. The slight roll off at the high-field end may be due to sample surface irregularities, because at these fields the pitch of the helical trajectory is approximately 10 μm. Small departures from the predicted field dependence are not surprising since Bloomfield's amplitude calculation is based on the assumption that the monotonic magnetoresistivity tensor elements have exactly the field dependence predicted by theory.[10,34] However, it is well known[35] that the "quadratic" magnetoresistance expected in compensated metals typically has a field dependence anywhere between $H^{1.8}$ and $H^{2.0}$. If all "quadratic" components actually were proportional to $H^{1.8}$, Bloomfield's theory would predict an $H^{1.1}$ dependence for the amplitudes, in better agreement with the data.

The behavior of P_4, on the other hand, is anomalous. The amplitude increases up to $H \approx 7$ kOe, then diminishes rapidly. The amplitude peak shifts toward larger fields as $\vec{H}$ is turned farther away from [0001]. Similar amplitude anomalies were observed for P_5–P_9. A striking example of this damping is shown in Fig. 14. The P_4 oscillations dominate below 6 kOe, while the P_1 oscillations dominate at larger fields and continue to increase

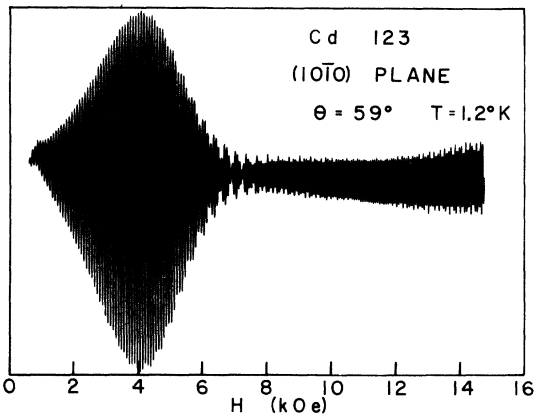

FIG. 14. Recorder tracing showing the damping of P_4 at higher fields. P_4 dominates below 7 kOe. P_1 dominates at higher fields. The slight irregularity at the high-field end is due to the weak P_{10} oscillations.

in amplitude to fields greater than 15 kOe. This indicates that the damping of P_4 is not due to irregularities of the sample faces since such irregularities presumably would have a similar effect on the P_1 oscillations, which have period (and therefore helix pitch) comparable to that of P_4. The possibility that the disappearance of P_4 arises from beating with another, nearly identical, period such as P_9 was eliminated by extending the field range to 20 kOe. The P_4 oscillations did not reappear as one would expect from the rapid drop in amplitude following the peak at 4 kOe.

We interpret the anomalous damping of the P_3–P_9 oscillations as an effect of magnetic breakdown between the first and second bands. Although breakdown has previously been observed only for carriers crossing the *AHL* plane or travelling in the ΓKM plane, it appears that tunneling can occur at other places on the monster. A cross section through the cap and monster in the ΓAHK plane is shown in Fig. 15. The shaded region on the right side of the drawing indicates where the valleys on the monster are very close to the edges of the cap. Since an electron crossing a valley must undergo Bragg reflection in order to continue on its orbit, it is likely that tunneling can occur at any point along the shaded region. Any orbit passing all the way around the monster column structure will therefore have at least three points of possible magnetic breakdown. We note that P_4–P_8 and, tentatively, P_9 have been assigned to orbits of this type. The only other period so assigned is P_3.

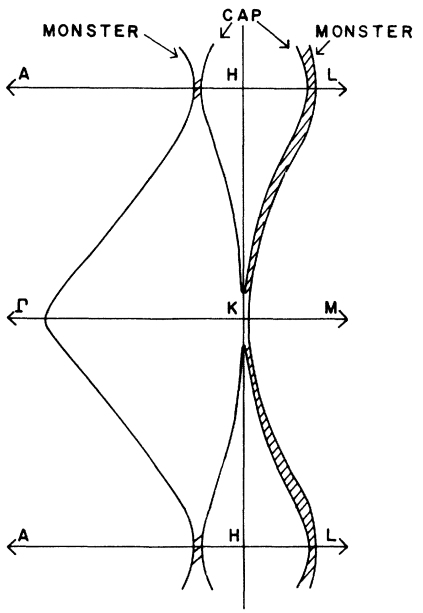

FIG. 15. Cross section through the cap and monster in the ΓAHK plane (Refs. 23 and 25). Shaded regions indicate where tunneling is likely to occur.

While the P_3 oscillations do in fact show slight damping in fields larger than 13 kOe (Fig. 3, lower trace), this could be due to surface irregularities. The remaining periods except perhaps P_{12}, which is unassigned, arise from orbits that do not involve reflection at the spin-orbit gap, and it is significant that these oscillations do not exhibit anomalous damping.

Calculation of the influence of magnetic breakdown on this semiclassical size effect is particularly straightforward. Because of the diffuse reflection at the sample surfaces, an electron just leaving the surface will be at an arbitrary point on its orbit in reciprocal space. However, magnetic breakdown can occur only at the Bragg-reflection points on the orbit. For this reason, the current carried by electrons that undergo magnetic breakdown while crossing the sample averages to zero, so the oscillatory conductivity is proportional to the probability that an electron crosses the sample without tunneling. When an electron reaches a Bragg point, the probability of tunneling is[36]

$$P(H) = e^{-H_0/H}, \tag{6}$$

where H_0 is the breakdown field. Since there may be several Bragg-reflection points on the orbit, each having a particular breakdown field, the probability that an electron survives its trip across the sample without tunneling is

$$S(H) = \prod_{i=1}^{m} [1 - P_i(H)]^{N(H)}, \tag{7}$$

where the $P_i(H)$ are the tunneling probabilities for the various Bragg points and $N(H)$ is the number of turns in the helical trajectory crossing the sample. Recalling that there is one oscillation for each turn and using Eq. (6), we find

$$S(H) = \prod_{i=1}^{m} (1 - e^{-H_i/H})^{H/P}, \tag{8}$$

where P is the period and $H_1 \ldots H_m$ are the breakdown fields of the various Bragg-reflection points.

In order to calculate the amplitude of the *resistivity* oscillations, we must take account of any modification of the monotonic galvanomagnetic properties induced by magnetic breakdown. In the case of cadmium, however, breakdown occurs between two hole surfaces, so the compensation of carriers is not affected. The monotonic terms therefore are unchanged by breakdown except when $\vec{H}$ is in the (0001) plane, where the open orbits on the monster break down to form closed orbits.[18,28] For field orientations out of the (0001) plane, the observed amplitude is therefore given by

$$A(H) = A_0 H^n S(H) = A_0 H^n \prod_{i=1}^{m} (1 - e^{-H_i/H})^{H/P}, \tag{9}$$

where n is the exponent predicted by Bloomfield for a given type of orbit (Table I) and A_0 is an amplitude factor which depends on temperature, sample thickness, purity, and Fermi-surface geometry. This expression indicates that the amplitude is unaffected at very low fields, where most electrons travel across the sample without tunneling, but begins to diminish at higher fields.

The field dependence of the P_4 amplitude was measured for several field orientations with considerable care taken to avoid systematic errors due to ac skin-depth problems in the samples or changes in modulation amplitude with field strength. Equation (9) was then fitted to the data, treating A_0, n, and the H_t as adjustable parameters. For all field directions studied, best fits were obtained by assuming that tunneling takes place at one point only on the orbit, implying that the breakdown field for one Bragg-reflection point is much smaller than for the others. In this case, Eq. (9) reduces to

$$A(H) = A_0 H^n (1 - e^{-H_0/H})^{H/P}, \qquad (10)$$

where H_0 is the breakdown field at the one point on the orbit where tunneling occurs. We first determined A_0 and n from the low-field data, where the amplitude has a simple H^n dependence, and then adjusted H_0 for agreement with the data at higher fields where the amplitude decays.

The data for $\theta = 65°$ are compared in Fig. 16 with curves obtained from Eq. (10) using three different values for H_0. The fit for $H_0 = 40$ kOe is quite good over a range of nearly a factor of 5 in amplitude. Data for four other field orientations are shown in Fig. 17, together with the best-fit theoretical curves from Eq. (10). One interesting feature of these curves is the rapid damping of the oscillations at magnetic fields much smaller than H_0. This results from the fact that at 10 kOe, for example, the oscillatory current arises only from those electrons which survive approximately 100 consecutive cycles around their orbit without tunneling. The best-fit values of H_0 are plotted vs θ in Fig. 18. (No breakdown data were taken in the range $59° < \theta < 63°$ because of interference from P_9.)

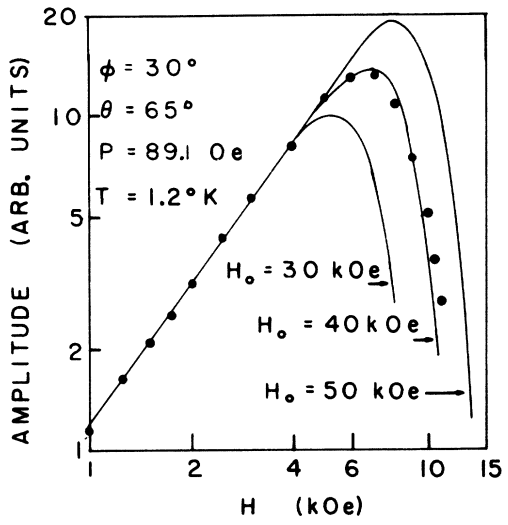

FIG. 16. Amplitude of P_4 oscillations vs magnetic field together with curves obtained from Eq. (10) assuming three different values of H_0. Dots: experimental points. Smooth curves: theory.

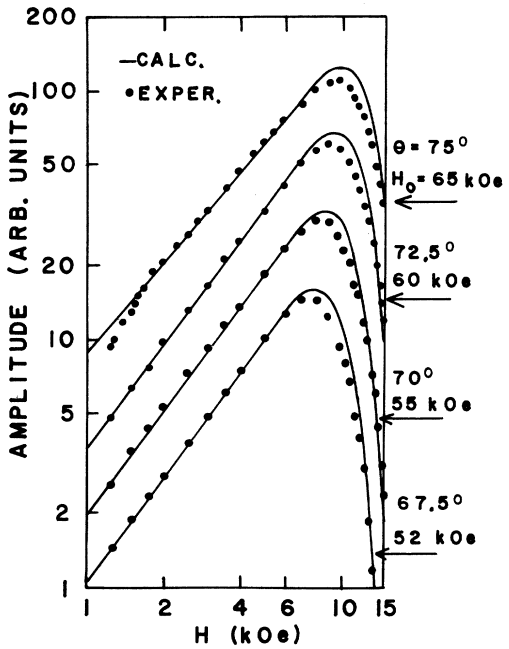

FIG. 17. Amplitude of P_4 oscillations vs magnetic field for four field orientations together with best-fit curves obtained from Eq. (10). Dots: experimental points. Smooth curves: theory.

Since the P_4 orbit traverses three valleys on the monster, there are three points at which carriers may tunnel to the first band [compare Figs. 2(b) and 10]. Because the data suggest that tunneling takes place predominantly at one point only on the orbit, we conclude that magnetic breakdown occurs at the bottom of one of the valleys (across the shaded region on the right side of Fig. 15). The precise location of this point cannot be determined because the position and shape of the orbit are only approximately known.

Other workers have reported values of H_0 ranging from a few kOe for the [0001]-directed open orbits[28] to about 30 kOe for the trifoliate orbit around the monster in the ΓKM plane.[22] These variations are not surprising since the breakdown field depends on the magnitude and direction of the electron velocity at the Bragg-reflection point. This variation of H_0 with orbit location and field direction is un-

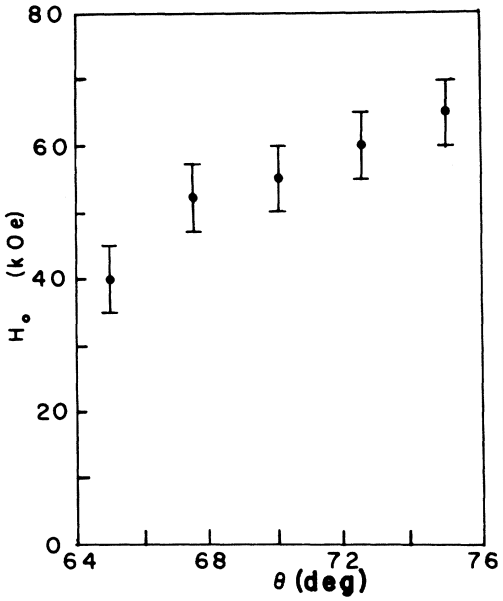

FIG. 18. Variation of H_0 with field direction in the $(10\bar{1}0)$ plane for the P_4 orbit.

doubtedly the reason why the P_3 oscillations do not exhibit anomalous damping.

V. SUMMARY

Several sets of size-effect oscillations were observed in cadmium for the first time, and those observed previously have been measured with greater accuracy over a larger range of field orientations. Most of the new oscillations have been assigned to extremal area-derivative orbits on the Fermi surface. The results indicate a slight departure of the third-band lens from axial symmetry about [0001].

The second harmonics of several oscillatory periods have been resolved clearly and are attributed in most cases to noncircular orbit geometry. It appears, however, that the second harmonic of the lens limiting-point oscillations may arise from specular reflection at the sample faces.

The anomalous damping of some but not all sets of oscillations at higher magnetic fields is attributed to the onset of magnetic breakdown of the gap between the first and second bands. A semiclassical model for the influence of magnetic breakdown is in reasonable agreement with the data, and the results suggest that the size effect is a useful tool for studies of magnetic breakdown using relatively small magnetic fields.

ACKNOWLEDGMENTS

It is a pleasure to thank R. W. Stark for making available the results of the Stark-Falicov Fermi-surface calculations and for assisting in the interpretation of the data. We also wish to acknowledge numerous helpful discussions with P. E. Bloomfield, J. A. Munarin, D. N. Langenberg, A. J. Arko, and J. E. Graebner.

*Research supported by National Science Foundation and by Advanced Research Projects Agency through the Materials Research Center of Northwestern University.

†Based on a thesis submitted by P. D. Hambourger in partial fulfillment of the requirement for the Ph.D. degree at Northwestern University.

‡Present address: Department of Physics, Cleveland State University, Cleveland, Ohio 44115.

[1]E. H. Sondheimer, Phys. Rev. **80,** 401 (1950).

[2]At the limiting point the plane tangent to the Fermi surface is normal to the magnetic field.

[3]Julius Babiskin and P. G. Siebenmann, Phys. Rev. **107,** 1240 (1957).

[4]N. H. Zebouni, R. E. Hamburg, and H. J. Mackey, Phys. Rev. Lett. **11,** 260 (1963).

[5]C. G. Grenier, K. R. Efferson, and J. M. Reynolds, Phys. Rev. **143,** 406 (1966).

[6]H. J. Mackey, J. R. Sybert, and J. T. Fielder, Phys. Rev. **157,** 578 (1967).

[7]V. L. Gurevich, Zh. Eksp. Teor. Fiz. **35,** 668 (1958) [Sov. Phys.-JETP **35,** 464 (1959)].

[8]J. A. Munarin and J. A. Marcus, *Proceedings of the Ninth International Conference on Low Temperature Physics, Columbus, Ohio*, edited by J. G. Daunt *et al.* (Plenum, New York, 1965), p. 743.

[9]P. Bloomfield, Bull. Am. Phys. Soc. **11,** 170 (1966).

[10]J. A. Munarin, J. A. Marcus, and Phillip E. Bloomfield, Phys. Rev. **172,** 718 (1968).

[11]P. D. Hambourger, J. A. Marcus, and J. A. Munarin, Phys. Lett. A **25,** 461 (1967); P. D. Hambourger and J. A. Marcus, Bull. Am. Phys. Soc. **13,** 43 (1968); Bull. Am. Phys. Soc. **14,** 400 (1969).

[12]H. J. Mackey, J. R. Sybert, and W. M. Waller, Phys. Rev. B **1,** 3979 (1970).

[13]V. P. Naberezhnykh and A. A. Maryakhin, Phys. Status Solidi **20,** 737 (1967).

[14]V. P. Naberezhnykh, Phys. Status Solidi **29,** K23 (1968).

[15]V. P. Naberezhnykh, N. K. Danshin, and L. T. Symbal, Zh. Eksp. Teor. Fiz. **55,** 389 (1968) [Sov. Phys.-JETP 28, 203 (1969)].

[16]R. G. Chambers, in *The Physics of Metals*, edited by J. M. Ziman (Cambridge U. P., Cambridge, England, 1969), p. 191.

[17]W. A. Harrison, Phys. Rev. **118,** 1190 (1960).

[18]N. E. Alekseevskii and Yu. P. Gaidukov, Zh. Eksp. Teor. Fiz. **43,** 2094 (1962) [Sov. Phys.-JETP **16,** 1481 (1963)].

[19]H. J. Mackey and J. R. Sybert, Phys. Rev. **158,** 658 (1967).

[20]H. J. Mackey and J. R. Sybert, Phys. Rev. **168,** 962 (1967).

[21]S. B. Soffer, Phys. Rev. B **3,** 1879 (1971).

[22]D. C. Tsui and R. W. Stark, Phys. Rev. Lett. **16,** 19 (1966).

[23]R. C. Jones, R. G. Goodrich, and L. M. Falicov, Phys. Rev. **174,** 672 (1968).

[24]R. W. Stark and L. M. Falicov, Phys. Rev. Lett. **19,** 795 (1967).

[25]R. W. Stark (private communication).

[26]R. G. Goodrich and R. C. Jones, Phys. Rev. **156,** 745 (1967).

[27]A. A. Galkin, E. P. Degtyar, S. E. Zhevago, and V. P. Naberezhnykh, Phys. Status Solidi **32,** K29 (1969).

[28]W. R. Datars and J. R. Cook, Phys. Rev. **187,** 769 (1969).

[29]P. D. Hambourger, Ph.D. thesis (Northwestern University, Evanston, Illinois, 1969) (unpublished).

[30]We thank H. J. Mackey for suggesting the use of this cleaning

method.
[31]R. W. Stark and L. R. Windmiller, Cryogenics **8,** 272 (1968).
[32]D. C. Tsui and R. W. Stark, Phys. Rev. Lett. **19,** 1317 (1967).
[33]H. Schwarz, Phys. Kondens. Mater. **9,** 1964 (1969).
[34]I. M. Lifshitz, M. Ia. Azbel', and M. I. Kaganov, Zh. Eksp. Teor. Fiz. **31,** 63 (1956) [Sov. Phys.-JETP **4,** 41 (1957)].
[35]E. Fawcett, Adv. Phys. **13,** 139 (1964).
[36]R. W. Stark and L. M. Falicov, in *Progress in Low Temperature Physics,* edited by C. J. Gorter (Wiley, New York, 1967), Vol. 5, p. 235.

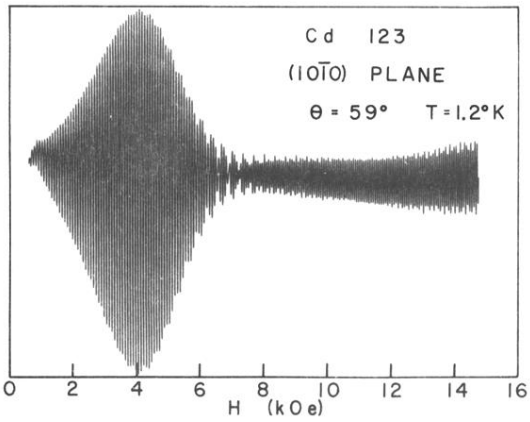

FIG. 14. Recorder tracing showing the damping of P_4 at higher fields. P_4 dominates below 7 kOe. P_1 dominates at higher fields. The slight irregularity at the high-field end is due to the weak P_{10} oscillations.